Experimental Investigation of Velocity Coupling in Combustion Instability

Y. Ma,* W. K. Van Moorhem,† and R. W. Shorthill‡
University of Utah, Salt Lake City, Utah 84112

An investigation has been conducted of the velocity coupling phenomenon reported in acoustically unstable solid-propellant rocket motors. An innovative simulation facility has been built using solid carbon dioxide as the simulated propellant. Acoustic disturbances are introduced over the dry-ice surface by means of a mechanically driven piston. Experiments have been conducted with dry ice located near both a velocity antinode and a velocity node. Mass flow rate and acoustic pressure measurements indicate the existence of a coupling mechanism, strongly dependent on the acoustic velocity amplitude, between the acoustic disturbance and the dry-ice sublimation process. Flow visualization and hot-film anemometry both show that the flow is turbulent near resonance. Transition to turbulence near a velocity node appears to occur at a smaller critical acoustic velocity amplitude than that near a velocity antinode. Some preturbulent instability has also been observed. Acoustically induced, turbulent forced convection is believed to be responsible for the increase in the sublimation rate of the dry ice (simulated burning of the propellant). Turbulence is believed to be one of the principal mechanisms in the velocity coupling phenomenon. An empirical correlation was developed which appeared to apply to the real propellant cases.

Introduction

ACOUSTIC combustion instability in solid-propellant rocket motors has been studied for more than 20 years. The major energy-generation mechanism in combustion instability is the unsteady combustion of the propellant. The interaction between the flowfield above the burning propellant and the combustion process is clearly a complicated nonlinear process, but instability theories generally use simplified linear models. The most generally accepted relationship between the propellant burning rate and the flowfield is termed pressure coupling. In this model, the unsteady burning rate of the propellant is taken to be proportional to the pressure oscillations. Pressure coupling is mainly determined by the thermal-chemical properties of the burning propellant and is reasonably well-understood. Some investigators[1,2] believe that the combustion process is also sensitive to velocity oscillations parallel to the propellant surface, velocity coupling. Velocity coupling is somewhat controversial. It would have to depend on instantaneous local flow conditions within the acoustic boundary layer and the heat transfer between the flow and propellant surface. Recent numerical studies of Beddini and Roberts[3,4] suggest that transition of the acoustic boundary layer above the propellant surface into turbulence could be one of the principal mechanisms of velocity coupling.

Brown and his co-workers[5–8] have attempted to investigate the heat transfer associated with turbulence in a cold flow simulation of the flow in a solid-propellant motor. They, however, focused on the transition of the mean flow rather than the acoustically induced transition and on the oscillating heat transfer in the presence of mean flow transition. As is discussed below, this is not the effect that appears to control velocity coupling.

Ma et al.[9,10,11] have reported previous experimental investigations of the velocity-coupling phenomenon using simulation techniques. Dry ice [solid carbon dioxide (CO_2)] was used in a piston driven chamber to simulate the combustion of a propellant. The fluid dynamic aspect of the problem was separated from the combustion process by this technique. Transitional behavior has been observed within the flow over the transpiring dry-ice surface in large-amplitude acoustic oscillation cases using both flow-visualization and hot-film anemometry techniques. An increase in the mean sublimation rate has also been measured, which appears to be caused by the increased heat transfer due to turbulent forced convection. A velocity type of coupling mechanism was suggested to exist as a result of the experiments, and turbulence appeared to be the principle mechanism in the coupling process.

The previous experiments, however, were conducted with the dry ice located near a velocity node and the increase in the mean sublimation rate of the dry ice could be argued to exist as a result of a nonlinear pressure-coupling mechanism. It is therefore of great interest to conduct similar experiments with dry ice located near a velocity antinode. In addition, some modifications have been made to the design of the section that contains the dry ice. These modifications appears to have influenced some of the previous results.[12] In the present study, experiments have been conducted with the dry ice located located near both a velocity antinode and a velocity node using the modified dry-ice section. Hot-wire anemometry and flow visualization have again been used to investigate the occurrence of turbulence within the flow over the simulated propellant.

Experiment

Figure 1 is a schematic diagram of the Solid-Propellant Rocket Motor Simulation Facility. The central part of the system was a chamber about 6-ft long, consisting of six interchangeable modular sections. The chamber was bolted down to a heavy granite table to minimize vibration. The inner cross section of the chamber was a 3-in. square. One of the chamber sections was designed to contain the dry ice (see Fig. 2). This section could be moved to different positions in the chamber.

Presented as Paper 90-0038 at the 28th Aerospace Sciences Meeting, Reno, NV, Jan. 8–11, 1990; received Jan. 22, 1990; revision received July 1, 1990; accepted for publication July 16, 1990.

*Graduate Research Associate, Mechanical Engineering Department; currently with IOMEGA Corp., Roy, UT 84067. Member AIAA.

†Associate Professor, Mechanical Engineering Department. Member AIAA.

‡Research Associate Professor, Mechanical Engineering Department. Member AIAA.

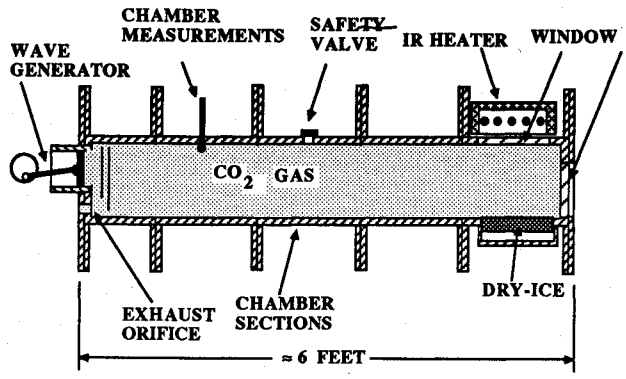

Fig. 1 Schematic diagram of experimental apparatus.

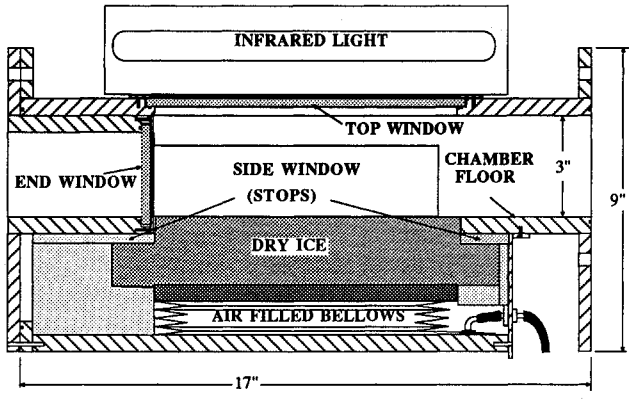

Fig. 2 Schematic diagram of the dry-ice section.

In the current study, two locations have been used. First, the dry-ice section was placed near the center of the chamber, where the acoustic velocity was a maximum while the pressure was a minimum. This setup minimized the pressure type of coupling in the dry-ice sublimation. Second, experiments have also been conducted with dry ice located at the upstream end of the chamber, where turbulence was generally considered least likely to occur.

There were four quartz windows on the dry-ice section. The top window allowed externally generated infrared radiation to reach the dry-ice surface and increase the sublimation rate or injection Mach number. An infrared lamp with 4.8 kW maximum power input was located above the dry-ice section. The output from the heat lamp was fairly uniform over the surface with a maximum deviation in intensity of about 4%. The two side windows and the end window were for viewing the flow or could be replaced with metal plates allowing a pressure and/or velocity probes to be introduced. The dry ice used had a 3×9-in. rectangular surface area and initially was about 1.5 in. thick. Commercial dry ice has been used in this study. During the experiment, the dry ice was supported by an air bellows, which was connected to a pressure-regulated air supply. The dry ice was pushed against two stops by the air bellows, keeping the dry-ice surface flush with the inner chamber surface as the dry ice sublimed. A constant 3 psi bellows supply pressure has been used in all of the experiments, which has been chosen to be large enough so that oscillatory acoustic pressure on the dry-ice surface would not cause significant vibration of the dry-ice block. The dry ice could be replaced with a fitted aluminum plate, which made the investigation of the flowfield without injection possible. Before each experiment, the chamber was purged with a room temperature CO_2 gas.

The CO_2 gas was allowed to exit the chamber through an orifice at the downstream end. A piston of 5-in.^{3} volumetric displacement, driven by a variable speed electric motor, was also mounted on the downstream end plate. The piston was used to produce a strong acoustic oscillation inside the chamber. Since the piston motion was not pure sinusoidal, the gas inside the chamber could be excited when piston was running at one-third or one-half of the fundamental natural frequency of the chamber. A pressure transducer (Kistler 606L) was mounted at the upstream end to monitor the pressure oscillation. The mean flow rate of the CO_2 gas from the chamber was measured with a Dwyer rotometer type flow meter, which was connected to the exit orifice. The mean pressure inside the chamber was also measured using a water manometer.

Flow visualization was conducted using a standard video camera (30 frames/s). A smoke-like "fog layer" over the dry-ice surface resulting from a small amount of water (less than 1% by weight) premixed within the dry ice during its manufacturing process provided an excellent means of visualization. During the flow visualization, the camera was focused on the center of the dry-ice section through one of the side windows.

In an attempt to determine if flow that appeared turbulent in the visualization was truly turbulent, a hot-film probe (TSI 1210-60) was used to sense the velocity fluctuations. One of the side windows was replaced with an aluminum plate through which the probe was inserted into the chamber. Because of the size of the probe-mounting base, the hot-film probe was located about 1 cm above the center of the dry-ice surface, as close to the surface as possible. Since the primary use of the hot-film probe here was to qualitatively examine the occurrence of turbulence in the flow, the location of the probe was therefore less important. Previous experiments over nontranspiring surfaces such as the work of Hino et al.[13] have shown that turbulence is diffused into entire flowfield from the boundary layer once transition occurs. In the current study, turbulence could also be convected into the entire flowfield due to surface injection. Hot-film measurements were made with the probe-sensing element perpendicular to the dry-ice surface. The output of the hot-film signal was displayed both on a digital oscilloscope (Nicolet 2090-II) and a spectrum analyzer (Hewlett Packard 3582A). Hardcopies of the output of the oscilloscope and spectrum analyzer were obtained using a X-Y recorder (Hewlett Packard 7046B).

At each dry-ice section locations, three different experiments were conducted: 1) dry ice was replaced with an aluminum plate; 2) dry ice was used and infrared radiation source operated at maximum power; and 3) dry ice was used and infrared radiation source was turned off.

Results and Discussion

Acoustic Pressure Measurement

Figure 3 shows the acoustic pressure amplitudes measured at the head end vs the piston-driving frequency for different setups. Small peaks observed at piston-driving frequencies of about 23 Hz and 34 Hz are due to the excitation of the fundamental acoustic mode of the chamber by the second or first harmonic of the piston motion when the piston is operated at one-third or one-half the frequency of the fundamental acoustic mode. A sharp increase in the pressure amplitudes is observed near resonances for all cases, as expected. In some cases, full resonance cannot be obtained with the present electric motor. The strong shock waves that occur near resonance limit the driving frequencies. The power output of the electric motor is too small to overcome the pressures associated with the shock.

An extremely interesting observation is that when the dry-ice section is located near the center, a velocity antinode, the acoustic pressure amplitude near resonance is largest in the case with dry ice and infrared radiation, smaller in the case with dry ice but without infrared radiation, and smallest in the case without dry ice. However, when the dry-ice section is location at the head end, a velocity node, this order is almost reversed. The pressure amplitude is largest in the case without dry ice and smaller and about equal in the cases with dry ice.

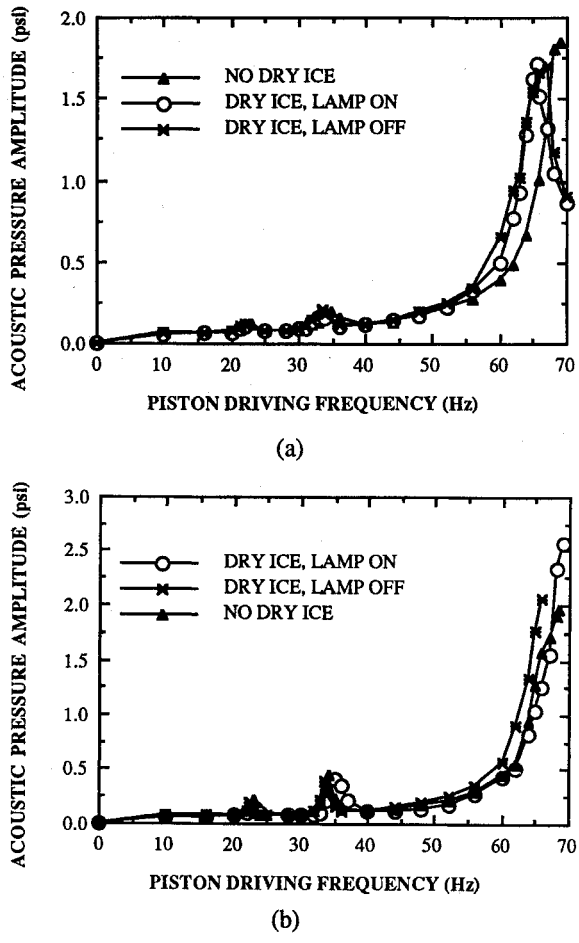

Fig. 3 Pressure amplitudes vs piston-driving frequency: a) dry ice at head end; and b) dry ice near center.

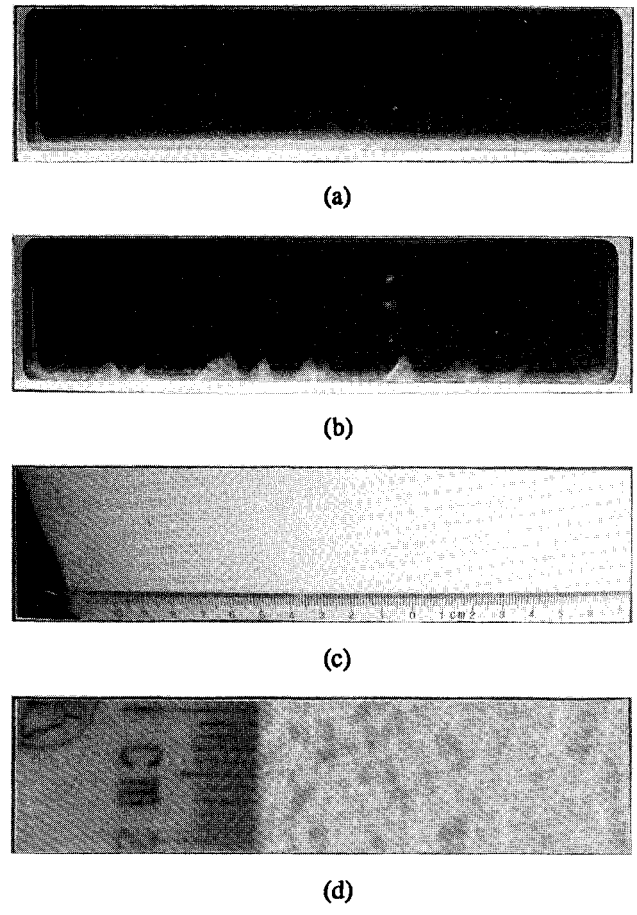

Fig. 4 a) Stable "fog" layer; b) wavy "fog" layer; c) smooth dry-ice surface, before experiment; and d) rough dry-ice surface after experiment.

Therefore an acoustic driving mechanism, related to the velocity oscillation and the dry-ice sublimation process, must exist.

Flow Visualization

Under steady-state operating conditions, i.e., no acoustic oscillation, a fairly uniform layer of "fog" can be clearly observed to form over the dry-ice surface as soon as the infrared radiation is applied. Figure 4a shows a stable "fog" layer. When a pressure disturbance is introduced over the dry-ice surface at low frequencies, the layer of "fog" is observed to pulsate up and down uniformly, responding to the simple compression of the gas. As the piston frequency increases, the amplitude of the "fog" layer pulsation decreases. It eventually becomes visually stationary when the piston reaches about 10 Hz. The "fog" layer remains stationary until a critical value of acoustic disturbance amplitude is reached. The flow within the chamber before the threshold condition definitely is laminar and stable. The values of this critical acoustic oscillation amplitude and the unsteady flow patterns are different for different dry-ice locations.

In the case where dry ice is located near the center of the chamber, instability is observed to occur within the "fog" layer at an acoustic Reynolds number (defined as $Re_a = U/(f\nu)^{1/2}$, where U, f, and ν are the amplitude of the acoustic velocity at the center of the dry ice, the piston-driving frequency, and the kinematic viscosity, respectively), of about 110. At the initiation of the instability, the "fog" layer exhibits a pattern of gradually varying hills and valleys or a wave-like pattern. The amplitude of the wave-like pattern increases as acoustic excitation becomes stronger. This wave-like pattern also exhibits a propagational behavior very similar to that of water waves. The "waves" propagate in both upstream and downstream directions from the center of the dry ice. However, the waves associated with the "fog" layer are extremely two-dimensional with the wave front observed to be very uniform across the width of the chamber. The flow appears to be mostly laminar or near the transition to turbulence. Figure 4b shows this type of wave motion observed with the "fog" layer.

At an acoustic Reynolds number of about 150, weak bursts of particles can be observed to leave the surface indicating local high-intensity instability. The smooth two-dimensional wave propagation no longer occurs. The waves break in a manner very reminiscent to the breaking of high-amplitude water waves. The process of transition to turbulence is believed to be taking place. A very interesting phenomenon is observed when the acoustic disturbance amplitude is further increased. The breaking wave fronts rise vertically, forming a series of vertical "fog" ridges that are amazingly uniform across the width of the chamber. This type of wave form also propagates in both upstream and downstream directions from the center. The tip of the "fog" slightly inclines towards the direction of the propagation and rolls as it travels, forming transverse vortices. When the acoustic Reynolds number is about 230, the "fog" layer motion no longer has any apparent pattern and is three-dimensional. This flow is believed to be turbulent.

At acoustic Reynolds number of about 450 (near chamber resonance), the fog layer is no longer visible due to increased mixing. However, the presence of a large number of particles ejected from the dry-ice surface indicates a very turbulent motion within the flow above the dry-ice surface. A possible explanation of these ejected particles is that they result from turbulent bursts associated with "wall" turbulent shear flow (see Hinze[14]). These particles are randomly ejected from the

surface in all directions. Nevertheless, most of them seem to follow paths inclined towards the downstream direction. The particles also tend to follow the acoustic oscillations as they leave the surface, exhibiting a longitudinal sinusoidal motion along the main trajectories. The particles can also be seen to bounce off the side walls of the chamber making it very difficult to follow the particle trajectories for long distances. These small particles are observed in all parts of the dry-ice section and the effects observed reach a maximum at resonance. Secondary motion of the particles can also be observed near the dry-ice surface. Here particles are seen to move in the downstream direction along the surface, towards the pressure antinode. This phenomenon likely indicates the influence of the acoustic streaming, where a net flow circulation occurs with the flow near surface moving from the velocity antinode towards the pressure antinode. Occasionally, large pieces of dry ice are observed to break off from the dry-ice surface due to the large shear stresses that occur. These large pieces of dry ice are not ejected from the surface nor do they attempt to follow the acoustic oscillation as the small particles do. However, the large pieces of dry ice do move in the streaming direction.

In the case where dry ice is located at the head end, however, the initial instability occurs at a much smaller acoustic Reynolds number of about 30. Moreover, the "fog" layer only exhibits a weak water wave-like motion, i.e., the propagation of wave motion is not two-dimensional and planar as in the previous case but rather appears to be radially outward from the center of the dry ice. Further increase in acoustic amplitude (Re_a = 55) causes the "fog" layer motion to become three-dimensional, random, and swirling. The "fog" layer again becomes invisible at very large acoustic Reynolds number (about 340) due to intense mixing. Visualization at this point then relies on the particles ejected from the surface.

The motion associated with the particles in this case is very similar to that observed when the dry ice is located near the center. The major difference is the direction of the secondary particle motion near the surface. The particles and the occasionally observed large dry-ice pieces are seen to travel in the upstream direction. This is consistent with the secondary motion due to acoustic streaming, since the upstream end of the chamber is the pressure antinode in this case. The flow near resonance is again very random and turbulent.

When the dry ice is located at the head end, the effect of surface roughness is very evident. A rough surface can be easily achieved by letting a piece of smooth dry ice run at the full resonant condition for short time. Figures 4c and 4d show typical surfaces of a dry-ice block before and after experiment. When the surface is rough, instability can be observed to occur at acoustic Reynolds number of about 20. The "fog" layer exhibits a pattern with randomly distributed small peaks. These peaks are very smooth and appear to result from overshooting or jetting of the "fog" due to local high sublimation rate. The "fog" jets are fixed in location. Each jet seems to form a small vortex as the tip of the jet moves towards downstream direction and falls back toward the surface at the same time. No wave-like motion is seen to propagate over the surface.

As the acoustic Reynolds number increases, the height of the jetting also increases, indicating stronger response of the sublimation process to increasing acoustic oscillation amplitude. Mixing eventually occurs within the flow at an acoustic Reynolds number of about 40 with the motion associated with the "fog" becoming three-dimensional and random, indicating a turbulent flow condition. The "fog" will no longer be visible at larger acoustic Reynolds numbers. The motion associated with the ejected particles is very similar to that when the surface is smooth.

The distinguishing characteristic of the flow pattern in this case is the dominance of the local instability. The preturbulent instability is very localized, random in location, and does not propagate into neighboring regions as compared to the highly organized and propagative flow pattern observed with dry ice located near the chamber center. A possible explanation is that near a velocity antinode, the gas motion is very uniform due to the small velocity amplitude gradient and is less influenced by any initial turbulence due to the higher velocity amplitude. Near the velocity node, however, the velocity amplitude is small and a strong velocity gradient also exists, allowing the instability to be localized and random. The strong velocity gradient will also cause nonuniform response of the dry-ice sublimation process, creating initial turbulence. Another indication of this type of mechanism is the fact that surface roughness appears to make no significant difference in the flow pattern observed when dry ice is located near the center.

Experiments conducted with the piston operating at full resonance show that the surface of the dry ice regresses faster where the acoustic velocity is expected to be higher. Therefore the upstream end of the dry-ice surface regresses faster than the downstream end with dry ice located just downstream of the center, while the opposite happens with dry ice located near the head end. This observation is in general agreement with the experiments of Crump and Price.[15,16]

In all situations, whenever there is an indication of approaching instability or of instability, an increase in the mean sublimation rate is observed. This enhanced sublimation can occur even while the flow appears to be laminar.

Hot-Film Anemometry

Occurrence of turbulence can also be determined by observing the spectrum of the hot-film output while varying the

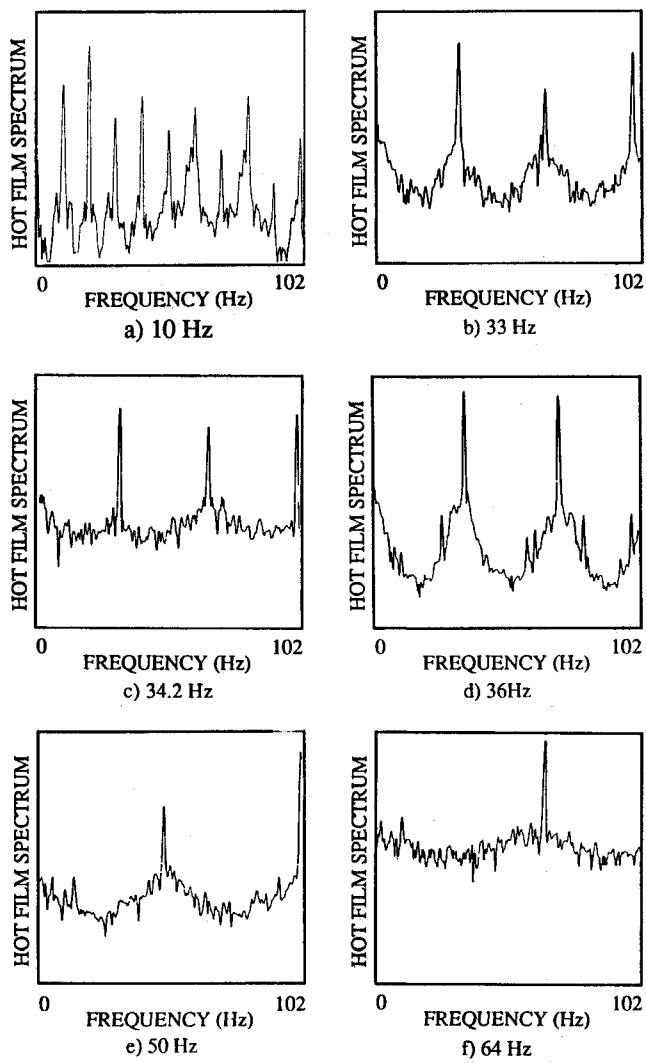

Fig. 5 Hot-film spectra with dry ice near the center.

piston-driving frequency. A broadband spectrum will indicate the occurrence of turbulence.

Figure 5 shows a series of spectra at different driving frequencies with dry ice located near the center of the chamber. The spectrum at 10 Hz shows only the harmonics of the piston-driving frequency, indicating a laminar flow condition. It can be observed that transition occurs at about 33 Hz, 36 Hz (with turbulent flow between these frequencies), and again at about 50 Hz, since the spectra at these frequencies starts to exhibit broadband behaviors. The same procedure has been applied to the case where dry ice is located near the head end of the chamber, and the results are shown in Fig. 6. Since the acoustic velocity amplitude is much smaller near the upstream end, transition appears to occur only at about 52 Hz. These findings again are in general agreement with the flow visualization, where turbulence is observed near one-half of the fundamental natural frequency of the chamber when dry ice is located near the center, while the flow only exhibits some preturbulent instability at one-half of the natural frequency with dry ice at head end.

Mass Flow Measurement

Figure 7 shows the measured mean volume flow rate vs the driving frequency of the piston for four cases (two dry-ice locations and with or without the infrared radiation). In the cases of no acoustic oscillation, the steady-state mean flow rates are the same for the two locations with infrared radiation. The flow rates are lower but also the same for the two locations without external heat addition. The difference between these situations is caused by the infrared radiation. At low piston-driving frequencies, no increase in the mean flow rate has been observed in any case. An increase in the flow rate has been recorded when the piston speed is about one-third of the fundamental natural frequencies of the chamber in the cases where the dry ice is located near the center of the chamber. An increase in the dry-ice sublimation rate has also been observed near one-half of the natural frequencies for all four cases. However, the amount of increase in the sublimation rate is always higher when the dry ice is located near the center of the chamber. A dramatic increase in the flow rate has been measured when the piston frequency is near the fundamental natural frequency of the gas in the chamber. Again the maximum flow rates measured are higher when the dry ice is located near the center. The nearly horizontal line on Fig. 7 is a calculated flow rate change vs frequency based on the thermodynamics property of the dry ice and the measured change in the mean chamber pressure for the cases with infrared radiation.

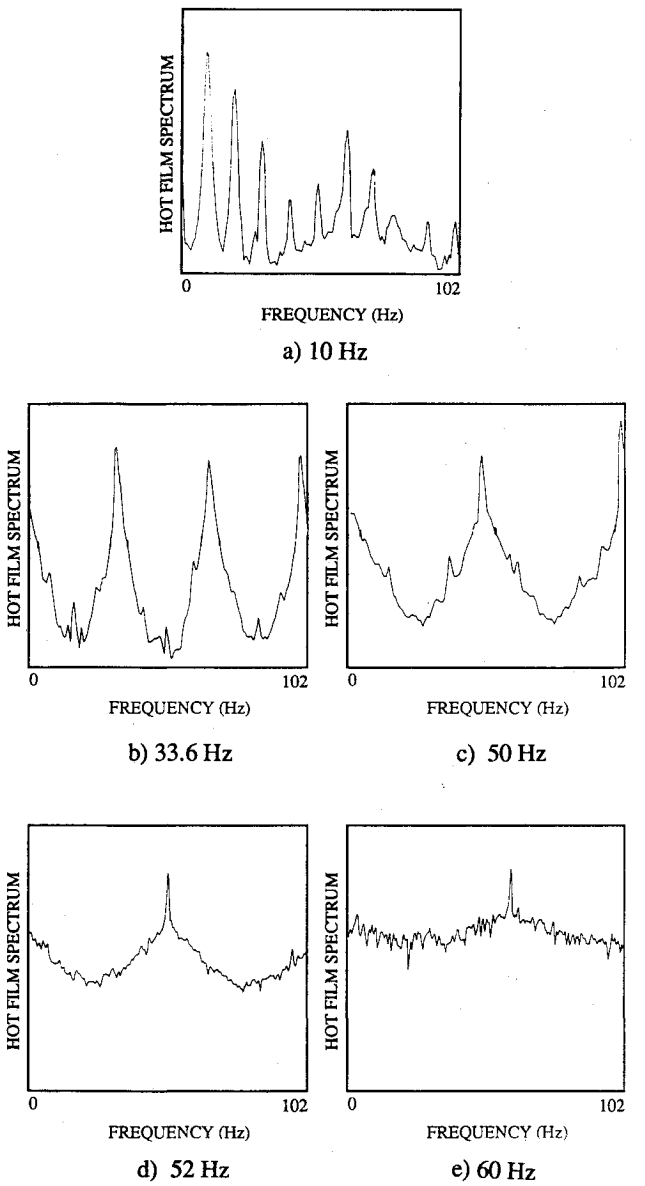

Fig. 6 Hot-film spectra with dry ice at head end.

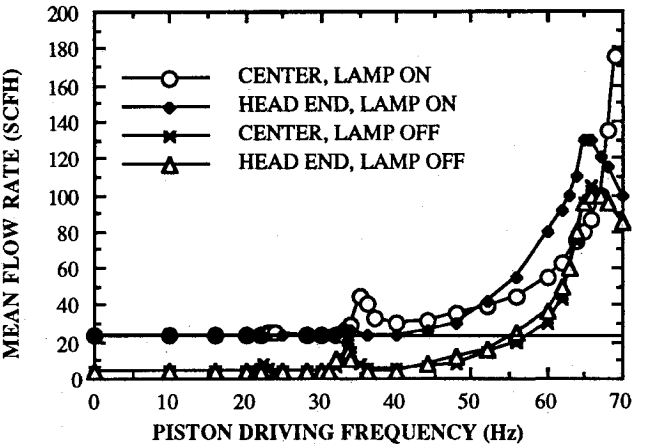

Fig. 7 Dry-ice mean flow rate vs piston frequency.

A comparison of Figs. 3 and 7 indicates that an increase in the dry-ice sublimation rate accompanies the increase in the acoustic oscillation amplitude. Any pressure type of coupling has to be ruled out since acoustic pressure amplitude is very small near a velocity antinode, where a larger increase in dry-ice sublimation rate is observed. A nonlinear effect such as thermal-acoustic heating[17] is very unlikely to be responsible for the increase in sublimation rate, since this mechanism increases with the strength in the shock wave and the shock is very weak near the chamber center even at resonance. Moreover, this effect has been observed to act like a heat pump; it cools the boundary at a velocity antinode while it transfers energy to the pressure antinode. Acoustic streaming, on the other hand, may contribute to the increase in the mass flow rate, since it results in a mean circulation of flow from velocity antinode to pressure antinode along the surface, which in turn can trigger a steady-state erosive burning type of phenomenon. However, the distribution of the streaming velocity amplitude is very similar to that of a second acoustic mode, i.e., the streaming velocities at both ends of the chamber and the center are zero. Therefore, it should be expected that the effect of acoustic streaming is similar in all of the cases with dry ice, since the relative location of the dry ice and the streaming velocity zeros is almost identical in all cases. It is also not clear how a second, order effect such as acoustic streaming may feed energy into first-order acoustic wave motion based on the classic acoustic streaming theory.

A velocity type of coupling mechanism is physically more reasonable. Figure 8 shows the mean sublimation rate as a function of the acoustic Reynolds number. The results show

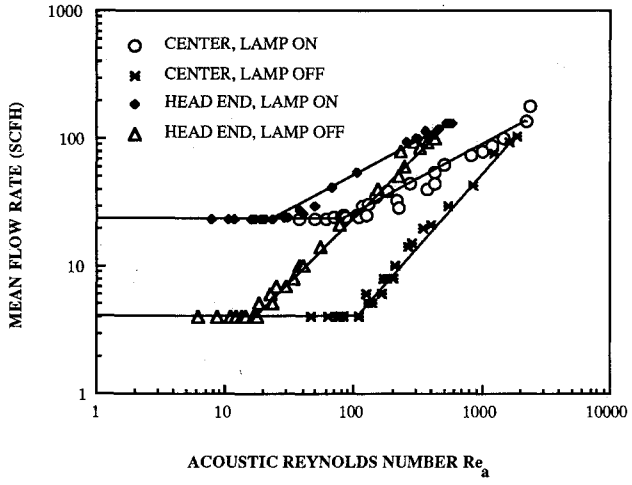

Fig. 8 Dry-ice mean flow rate vs acoustic Reynolds number.

a clear dependence of sublimation rate on the acoustic Reynolds number. In the cases of no infrared radiation, the sublimation of dry ice is dominated by the combination of natural convection and conduction effects at low acoustic excitation cases. The flow above the subliming dry-ice surface is laminar. However, as the acoustic velocity amplitude increases, the flow above the dry-ice surface becomes unstable. Transition to turbulence occurs as the acoustic Reynolds number reaches a critical value, which is indicated in the sharp increase in the sublimation rate. The heat-transfer mechanism is dominated by forced turbulent convection. Since the turbulence intensity increases with increasing acoustic disturbances, the sublimation rate increases with increasing acoustic oscillation amplitude.

In the cases where infrared radiation is applied over the dry-ice surface, the radiation heat-transfer mechanism dominates the weak natural convection and conduction effects in the laminar case, and a higher steady-state sublimation rate is therefore measured at low acoustic amplitude cases. As the acoustic disturbance increases, the flow again becomes unstable. Increases in the sublimation rate are observed as the heat convection to the dry-ice surface increases. The effect of turbulent convection increases and becomes dominant with increasing acoustic disturbance. The curves for the cases with and without infrared radiation appear to merge as the turbulent convection heat-transfer mechanism controls the sublimation process of the dry ice.

The threshold values of acoustic velocity amplitude at which the dry-ice sublimation rate starts to increase are about a factor of two less in the cases with dry ice located at heat end than at the center, indicating possible difference in the triggering mechanisms for the turbulence to occur as observed by flow visualization and hot-film anemometry.

A universal curve can be generated for this experiment by plotting the increased mean flow rate as a function of an increased acoustic Reynolds number ratio as shown in Fig. 9, where Re_{aini} is the acoustic Reynolds number at which initial increase in the dry-ice sublimation rate is observed. The data points for all four different experimental cases collapse nearly to a single curve, strongly supporting the dominance of the turbulent forced convection heat-transfer mechanism in the experiments. The scattering of data at low increased sublimation rate is due to the occurrence of preturbulence instability. Since the increased sublimation rate is proportional to the increased heat-transfer rate due to turbulent forced convection, this curve actually indicates a dependence of the turbulent heat-transfer rate in oscillatory flow to the amplitude of the oscillation. Curvefitting through all of the data yields an empirical relation

$$h \propto (Re_a/Re_{aini} - 1)^{0.8} \tag{1}$$

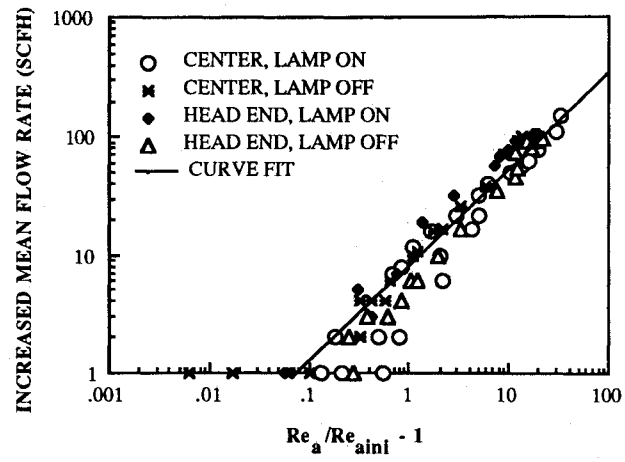

Fig. 9 Increased mean flow rate vs ratio of excessive acoustic Reynolds number.

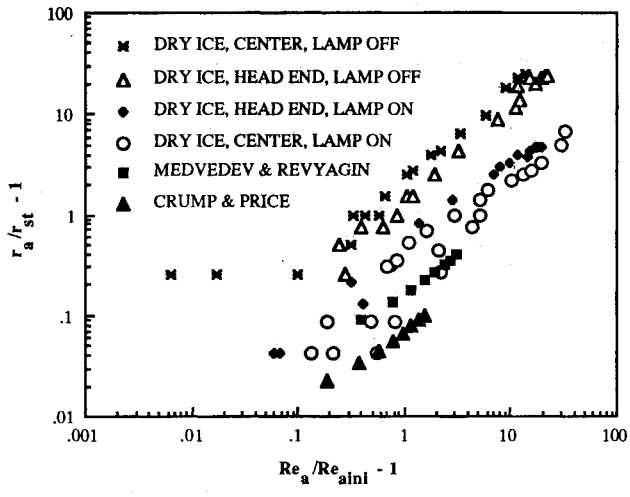

Fig. 10 Surface regression rate vs ratio of excessive acoustic Reynolds number.

where 0.8 is the slope of the curve in the log-log plot. This empirical relationship is very important since it provides a means of predicting the response of a subliming surface to acoustic oscillation in velocity coupling. Moreover, this correlation bears a striking similarity to the widely accepted convection heat-transfer correlation for fully turbulent nonoscillatory flow, where convection heat-transfer coefficient is expressed as

$$h \propto Re^{0.8}Pr^{1/3} \tag{2}$$

where Re is the steady flow Reynolds number ($Re = VD/\nu$) and Pr is the Prandtl number. This similarity again supports the occurrence of turbulence in the experiments. The dependence on Prandtl number has not been obtained since Pr is almost the same for all cases in this study.

Comparison with previous results of Crump and Price[15,16] and Medvedev and Revyagin[18] is possible by dividing the increased mean sublimation rate with the corresponding steady-state sublimation. The slopes of the data will not be affected by this operation when presented in log-log form. But the resulting ratio is the same as the increased regression rate that is used by these previous researchers in presenting their data. A striking similarity in the slopes of all experiments is observed and shown in Fig. 10. This suggests that the same mechanism (presence of turbulence or turbulent forced heat convection) is responsible for the increase of the mean burning rate of propellant in these previous experiments. The reason that all of these data do not fall into one curve here is due to the differences in the steady-state heat-transfer mecha-

nisms. However, the empirical relationship developed above appears to hold for all cases, i.e.,

$$r_a/r_{st} - 1 \propto (Re_a/Re_{aini} - 1)^{0.8} \quad (3)$$

where r_{st} and r_a are the steady-state surface regression rate and the surface regression rate due to acoustic disturbance.

The implication of the discussions in previous sections can be summarized as follows: 1) Energy in the acoustic waves has been increased as a result of the increasing sublimation of the dry ice (simulated increased burning rate of the solid propellant). 2) Heat is also transferred back to the simulated propellant surface due to an acoustic wave-induced mechanism. 3) The responsible coupling mechanism is believed to be related to the acoustic velocity oscillation and, most likely, the occurrence of turbulence.

Transition to Turbulence

It should be clear by now that the determination of the transition to turbulence is very important, since it will eventually enable the prediction of the response of the combustion process to velocity oscillation parallel to the propellant surface.

A comparison with the numerical results of Beddini and Roberts[3,4] is shown in Fig. 11, where U, V, f, and ν are the local acoustic velocity amplitude, the injection velocity at the wall, the piston-driving frequency, and the kinematic viscosity, respectively. The solid curve is the prediction of Beddini and Roberts. They predict turbulent flow for conditions above the curve and laminar below the curve. The experimentally determined transition regions are presented in several groups. The occurrence of turbulence has been determined by means of 1) flow visualization; 2) observing hot-film spectrum; and 3) flow rate measurement. These results agree fairly well with each other particularly for the cases where dry ice is located near the center.

It is seen that when the dry ice is located near the center, the experimentally determined critical Reynolds number is about 40% of that predicted by Beddini and Roberts.[3,4] The discrepancy may occur due to several reasons. First, the numerical prediction is based on the conditions that the wall is perfectly smooth and no initial turbulence exists due to the injection. In this experiment, the dry-ice surface does have a finite surface roughness and the surface injection rate may not be perfectly uniform, which may cause early transition to turbulence. Second, an isothermal condition has been assumed in Beddini and Roberts' analysis, while in our experiment a strong temperature gradient exists next to the dry-ice surface. However, no other theoretical results are presently available. Nevertheless, the experimental results seem to agree fairly well with the previous experimental work conducted over nontranspiring surface (see Ma[19]), where turbulence is seen to occur at acoustic Reynolds number ranging from 195–1000. The transition at the head end is considerably lower than the theory predicts, as have been discussed extensively in previous sections.

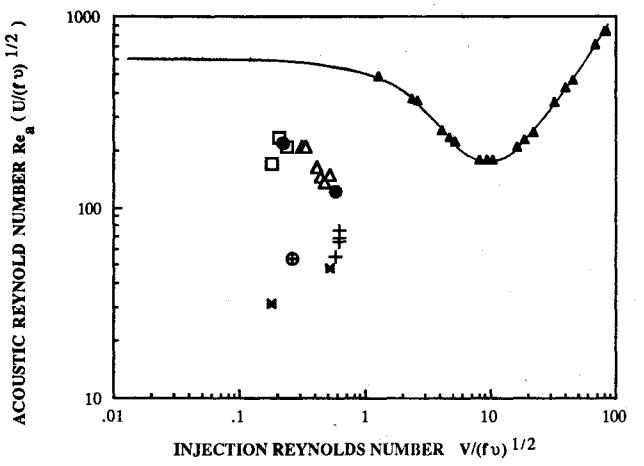

Fig. 11 Effect of surface injection on transition to turbulence. □: dry ice, center, hot film; △: dry ice, center, flow visualization; ●: dry ice, center, mean flow correlation; ○: dry ice, head end, hot film; +: dry ice, head end, flow visualization; ⋈: dry ice, head end, mean flow correlation; and ▲: Beddini and Roberts.

Conclusions

1) In this study, solid carbon dioxide was used as the simulated propellant to investigate the fluid dynamic aspects of the flow above a simulated burning propellant. This approach appears to be very successful since it reveals some very important characteristics associated with the oscillatory flow over transpiring surfaces.

2) Mean flow rate and pressure amplitude measurements show that a coupling mechanism appears to exist between the velocity component of the acoustic disturbance and the sublimation process.

3) Hot-film anemometry, flow visualization, and mean flow rate correlation all seem to indicate the transitional behaviors of the flow over the simulated burning propellant with increasing acoustic disturbance. The occurrence of turbulence is believed to play a very important role in the response of a propellant to velocity oscillations.

4) The influence of turbulence over excessive heat-transfer rate is seen to obey the ratio of an excessive acoustic Reynolds number to 0.8 power. This correlation appears to apply to propellant combustion cases and will be very important in future prediction of velocity coupling.

Acknowledgments

The authors would like to gratefully acknowledge the support of the U.S. Air Force Astronautics Laboratory through Contact FO4611-86-K-0083 and of the Thiokol Corporation, which made this work possible.

References

[1]Culick, F. E. C., "Stability of Longitudinal Oscillations with Pressure and Velocity Coupling in a Solid-Propellant Rocket," *Combustion Science and Technology*, Vol. 2, No. 4, 1970, pp. 179–201.

[2]Price, E. W., "Velocity Coupling in Oscillatory Combustion of Solid Propellants," *AIAA Journal*, Vol. 17, No. 7, 1979, pp. 799–800.

[3]Beddini, R. A., and Roberts, T. A., "Turbularization of an Acoustic Boundary Layer on a Transpiring Surface," AIAA Paper 86-1448, June 1986.

[4]Beddini, R. A., and Roberts, T. A., "Response of Propellant Combustion to a Turbulent Acoustic Boundary Layer," AIAA Paper 88-2942, July 1988.

[5]Brown, R. S., Willoughby, P. G., and Dunlap, R., "Coupling Between Velocity Oscillations and Solid-Propellant Combustion," AIAA Paper 84-0288, Jan. 1984.

[6]Brown, R. S., Blackner, A. M., Willoughby, P. G., and Dunlap, R., "Coupling Between Velocity Oscillations and Solid-Propellant Combustion," AIAA Paper 86-0531, Jan. 1986.

[7]Brown, R. S., Blackner, A. M., Willoughby, P. G., and Dunlap, R., "Coupling Between Velocity Oscillations and Solid-Propellant Combustion," Final Technical Rept., United Technologies Chemical Systems, Aug. 1986.

[8]Brown, R. S., Blackner, A. M., Willoughby, P. G., and Dunlap, R., "Coupling Between Velocity Oscillations and Solid-Propellant Combustion," *Journal of Propulsion and Power*, Vol. 2, Oct. 1986, pp. 428–437.

[9]Ma, Y., Heusser, E. J., Shorthill, R. W., and Van Moorhem, W. K., "A Simulation of the Flow Near a Burning Solid Rocket Propellant," AIAA Paper 89-0301, Jan. 1989.

[10]Ma, Y., Van Moorhem, W. K., and Shorthill, R. W., "Turbulence in an Acoustically Unstable Solid-Propellant Rocket Motor Simulation," AIAA Paper 89-2663, July 1989.

[11]Ma, Y., Van Moorhem, W. K., and Shorthill, R. W., "An Innovative Method of Investigating the Role of Turbulence in the Velocity Coupling Phenomenon," *Proceedings of the Symposium on Combustion Instabilities Driven by Thermo-Chemical Acoustic Sources*,

Vol. NCA-4/HTD-128, The American Society of Mechanical Engineers, 1989, pp. 17–22.

[12]Ma, Y., Van Moorhem, W. K., and Shorthill, R. W., "Results Due to Modification of the Dry-Ice Section—Addendum to 'An Innovative Method of Investigating the Role of Turbulence in the Velocity Coupling Phenomenon' Session NCA-2," ASME Winter Annual Meeting, San Francisco, CA, Dec. 1989.

[13]Hino, M., Sawamoto, M., and Takasu, S., "Experiments on Transition to Turbulence in an Oscillatory Pipe Flow," *Journal of Fluid Mechanics*, Vol. 75, Part 2, 1976, pp. 193–207.

[14]Hinze, J. O., *Turbulence*, 2nd ed., Chapter 7, McGraw-Hill Book Company, New York, 1975.

[15]Crump, J. E., and Price, E. W., "Effect of Acoustic Environment on the Burning Rate of a Double-Based Solid Propellants," *ARS Journal*, Vol. 31, No. 7, 1961, pp. 193–207.

[16]Crump, J. E., and Price, E. W., "Effect of Acoustic Environment on the Burning Rate of Solid Propellants," *AIAA Journal*, Vol. 2, No. 7, 1964, pp. 1274–1278.

[17]Merkli, P., and Thomann, H., "Thermoacoustic Effects in a Resonance Tube," *Journal of Fluid Mechanics*, Vol. 70, Part 1, 1975, pp. 161–177.

[18]Medvedev, Yu. I., and Revyagin, L. N., "Unsteady-State Erosion of a Powder," *Fizika Goreniya i Vzryva*, Vol. 10, No. 3, 1974, pp. 341–345.

[19]Ma, Y., "A Simulation of the Flow Near a Burning Propellant in a Solid-Propellant Rocket Motor," Ph.D. Dissertation, Department of Mechanical Engineering, Univ. of Utah, Salt Lake City, Utah, 1990.